ARTICLE

Enhanced circularly polarized luminescence of chiral Eu(III) coordination polymers with structural strain

Received 00th January 20xx,
Accepted 00th January 20xx

DOI: 10.1039/x0xx00000x

Makoto Tsurui, [a] Yuichi Kitagawa, [b] Sunao Shoji, [b,c] Koji Fushimi, [b] and Yasuchika Hasegawa *[b,c]

Three types of Eu(III) coordination polymers with different distorted chiral ligands, $[Eu(+tfc)_3(p\text{-dpeb})]_n$, $[Eu(+pfc)_3(p\text{-dpeb})]_n$, and $[Eu(+hfc)_3(p\text{-dpeb})]_n$ (+tfc: (+)-3-(trifluoroacetyl)camphorate, +pfc: (+)-3-(pentafluoropropionyl)camphorate, +hfc: (+)-3-(heptafluorobutyryl)camphorate, *p*-dpeb: 1,4-bis(diphenylphosphorylethynyl)benzene) were prepared for elucidating the relationship between their structural distortions, ligand-to-metal charge transfer (LMCT), and circularly polarized luminescence (CPL) properties. Their strain factors in the ligands were evaluated using crystallographic data obtained by single-crystal X-ray structural analyses. The characteristics of the LMCT excited states were estimated from theoretical calculations. The introduction of bulky substituent into the chiral ligand afforded a distorted structure of β-diketonates and changed the direction of the transition electric dipole moments, which are related to the magnitude of the CPL intensity. The CPL dissymmetry factor (g_{CPL}) of $[Eu(+hfc)_3(p\text{-dpeb})]_n$, with a large distorted structure, was −0.22, while those of $[Eu(+tfc)_3(p\text{-dpeb})]_n$ and $[Eu(+pfc)_3(p\text{-dpeb})]_n$, with small distorted structures, were −0.05 and −0.10, respectively. The controlled steric hindrance of the chiral ligands in Eu(III) coordination polymers is one of the strain factors for enhancing their CPL properties.

Introduction

Transition metal complexes with ligand-to-metal charge transfer (LMCT) or metal-to-ligand charge transfer (MLCT) states produce characteristic photofunctional properties such as photocatalytic activity,[1–6] solar cell efficiency,[7–9] and luminescence behavior.[10–13] Ritter provided the synthetic method of aryl fluoride from benzoic acids using LMCT excited states of a Cu(II) complex.[4] Moreover, Wenger recently reported characteristic MLCT luminescence from air-stable Mn(I) complexes with isocyanide chelate ligands.[13] The LMCT and MLCT states are directly related to the control of the photophysical and photochemical properties of transition metal complexes.

According to the trivalent lanthanide complexes, Jørgensen reported that the Eu(III) complex with dialkyldithiocarbamates showed a broad absorption band in the visible region, which was assigned to the LMCT band.[14] Generally, the LMCT states of Eu(III) complexes are produced by the electronic transition from the HOMO level of the ligand to the LUMO level of the Eu(III) ion.[14,15] The steric strain of the ligand may affect the energy level and direction of the transition dipole moment of the LMCT states in Eu(III) complexes (Figure 1a and 1b). Recently, we described that the relationship between the LMCT states in chiral Eu(III) compounds and their circularly polarized luminescence (CPL) properties.[16,17] In our previous paper, the substituents of chiral phosphine oxide ligands in Eu(III) complexes provided the structural strain in β-diketonate ligands, which affected the coordination geometries, LMCT, and CPL properties. We discussed on the strain-factor based on the crystal and ligand field (steric structure) for enhancement of LMCT and CPL bands.[16]

In this study, we focused on the electronic structure of the ligands based on the LMCT characteristics for evaluating the CPL properties of chiral Eu(III) compounds. From this concept, chiral Eu(III) coordination polymers with rigid and long linker ligands were selected. The linker ligands provide wide space for packing the bulky chiral ligands without crystal field change (Figure 1c). This molecular design allows us to understand the direct effect of ligand strain on the LMCT characteristics and the CPL properties.

Herein, we report on chiral Eu(III) coordination polymers with controllable distorted structures. These polymers are composed of chiral luminescent Eu(III) units and rigid linker parts. Three chiral ligands with perfluoroalkyl groups of different length, (+)-3-(trifluoroacetyl)camphorate (+tfc), (+)-3-(pentafluoropropionyl)camphorate (+pfc), and (+)-3-(heptafluorobutyryl)camphorate (+hfc), were selected to systematically control the strain factor in the Eu(III) coordination polymer (Figure 1d). The ethynyl-linked phosphine oxide, 1,4-bis(diphenylphosphorylethynyl)benzene (*p*-dpeb), was synthesized as a linear rigid linker to create a wide space to

[a] *Graduate School of Chemical Sciences and Engineering, Hokkaido University, Kita 13, Nishi 8, Kita-ku, Sapporo, Hokkaido 060-8628, Japan.*
[b] *Faculty of Engineering, Hokkaido University, Kita 13, Nishi 8, Kita-ku, Sapporo, Hokkaido 060-8628, Japan.*
[c] *Institute for Chemical Reaction Design and Discovery (WPI-ICReDD), Hokkaido University, Kita 21, Nishi 10, Kita-ku, Sapporo, Hokkaido 001-0021, Japan.*
E-mail: hasegaway@eng.hokudai.ac.jp

†Electronic Supplementary Information (ESI) available: Synthetic scheme, ESI-MS spectra, PXRD patterns, crystallographic data, emission spectra, temperature-dependent emission lifetimes, Arrhenius parameters, diffuse reflection spectra, theoretical calculations, CPL spectra and NMR spectra. CCDC 2213525 and 2213526. For ESI and crystallographic data in CIF or other electronic format see DOI: 10.1039/x0xx00000x

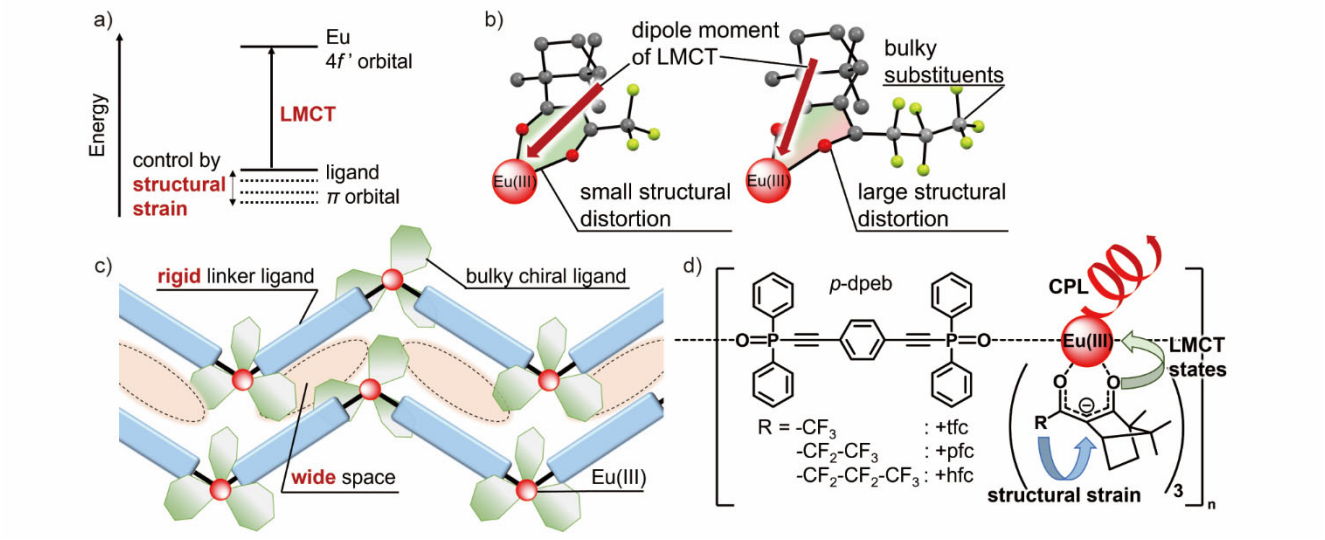

Figure 1. Illustrations of a) controlling the LMCT energy level, b) the direction of the dipole moments by structural strain, and c) the conceptual design of a chiral Eu(III) coordination polymer. d) Chemical structures of the chiral Eu(III) coordination polymers.

hold the large camphorate ligands (Figure 1c).[17,18] Three chiral Eu(III) coordination polymers, $[Eu(+tfc)_3(p\text{-dpeb})]_n$, $[Eu(+pfc)_3(p\text{-dpeb})]_n$, and $[Eu(+hfc)_3(p\text{-dpeb})]_n$ (Figure 1d) were synthesized using these ligands to tune the steric hindrance of the chiral ligands in the Eu(III) coordination polymers.

The coordination structures of the chiral Eu(III) coordination polymers were characterized by single-crystal X-ray structural analyses. The strain factors in the camphorate ligands were estimated from their crystallographic data. The photophysical properties of the Eu(III) coordination polymers were evaluated using the emission spectra, lifetimes, and CPL measurements. Time-dependent density-functional theory (TD-DFT) calculations were then carried out for estimation of the LMCT states. The large steric hindrance of the camphorate ligands provides characteristic interaction between LMCT states and 4f-4f excited states in Eu(III), resulting in effective CPL properties.

Results and discussion

Structural characterizations

Chiral Eu(III) luminescent centers were obtained by the reaction of Eu(III) acetate and chiral camphorate ligands (+tfc, +pfc, and +hfc) in methanol and water.[19] The chiral Eu(III) coordination polymers with diethynylbenzene linkers, $[Eu(+tfc)_3(p\text{-dpeb})]_n$, $[Eu(+pfc)_3(p\text{-dpeb})]_n$, and $[Eu(+hfc)_3(p\text{-dpeb})]_n$, were synthesized by complexation of *p*-dpeb with precursor chiral Eu(III) units in methanol and purified by recrystallization from ethanol solution (Scheme S1, ESI). The ESI-MS spectra and simulated mass patterns of $[Eu(+tfc)_3(p\text{-dpeb})]_n$ are shown in Figure S1 (ESI). The observed signals with mass numbers (*m/z*) of 1173.25, 2593.63, 4013.94, and 5434.32 were assigned to the $[Eu(+tfc)_2(p\text{-dpeb})]^+$, $[Eu_2(+tfc)_5(p\text{-dpeb})_2]^+$, $[Eu_3(+tfc)_8(p\text{-dpeb})_3]^+$, and $[Eu_4(+tfc)_{11}(p\text{-dpeb})_4]^+$ fragments, respectively. Assignments were made by comparing the observed isotope distribution of $[Eu_n(+tfc)_{3n-1}(p\text{-dpeb})_n]^+$ (*m/z* at approximately 1173.2, 2593.7, 4013.9, and 5434.2) with the calculated data. The observed ESI-MS signals of $[Eu(+pfc)_3(p\text{-dpeb})]_n$ and $[Eu(+hfc)_3(p\text{-dpeb})]_n$ were also assigned to the $[Eu_n(+pfc)_{3n-1}(p\text{-dpeb})_n]^+$ and $[Eu_n(+hfc)_{3n-1}(p\text{-dpeb})_n]^+$ fragments, respectively (Figure S2 and S3, ESI).

The powder X-ray diffraction (PXRD) patterns of the chiral Eu(III) coordination polymers are shown in Figure S4 (ESI). Characteristic sharp diffraction maxima were observed for each coordination polymer because of its high crystallinity. The single crystals of $[Eu(+pfc)_3(p\text{-dpeb})]_n$ and $[Eu(+hfc)_3(p\text{-dpeb})]_n$ were successfully obtained by recrystallization from ethanol solution and their structures were determined by single-crystal X-ray structural analyses. The crystallographic data are summarized in Figure 2a, 2b, and Table S1 (ESI). The space groups of these Eu(III) coordination polymers were categorized as $P2_12_12_1$, which is a chiral space group. The ORTEP views of these chiral Eu(III) coordination polymers exhibited eight-coordinated structures in which three chiral camphorate ligands and two phosphine oxide groups were coordinated to one Eu(III) ion. Two phosphine oxide groups in the *p*-dpeb ligand were attached with different Eu(III) ions to form the coordination polymer structure.

Based on their crystal data, we performed continuous shape measure (CShM) calculations using SHAPE[20–22] to determine the geometrical structures around the Eu(III) ions in the first coordination sphere (see ESI). The CShM factor (S_{CShM}) values obtained for these complexes for 8-SAP and 8-TDH (SAP: square antiprism, TDH: triangular dodecahedron) are summarized in Table 1. The S_{CShM} values in the 8-SAP structures are smaller than those of 8-TDH in the synthesized chiral Eu(III)

Table 1. S_{CShM} values of the chiral Eu(III) coordination polymers.

Compounds	S_{CShM} (8-SAP)	S_{CShM} (8-TDH)
$[Eu(+pfc)_3(p\text{-dpeb})]_n$	0.704	1.422
$[Eu(+hfc)_3(p\text{-dpeb})]_n$	0.526	1.433

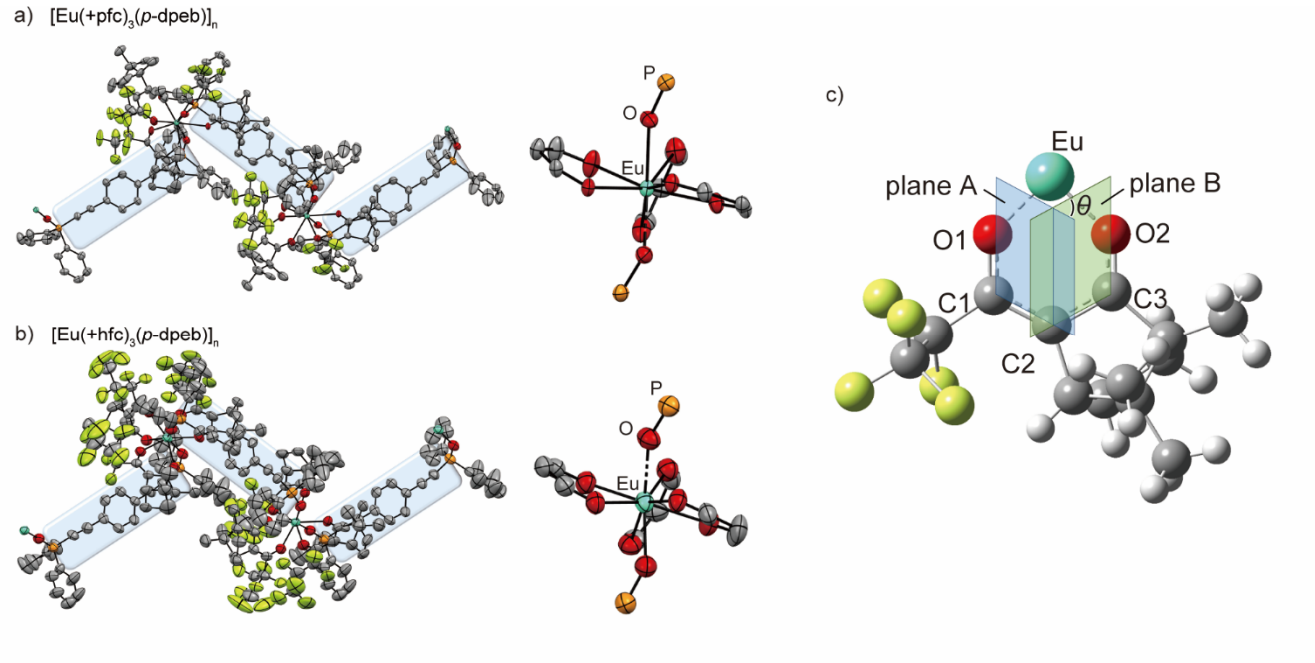

Figure 2. ORTEP drawings (ellipsoids set at 50 % probability, hydrogen atoms were omitted for clarity) of a) $[Eu(+pfc)_3(p\text{-dpeb})]_n$ and b) $[Eu(+hfc)_3(p\text{-dpeb})]_n$. c) Illustration of dihedral angle θ in camphorate ligand.

coordination polymers. Thus, the coordination geometries of $[Eu(+pfc)_3(p\text{-dpeb})]_n$ and $[Eu(+hfc)_3(p\text{-dpeb})]_n$ were categorized as 8-SAP.

To estimate the strain magnitude of the chiral Eu(III) coordination polymers, we focused on the orientation and planarity of the coordinated β-diketonate ligands. The orientation of the chiral ligands in $[Eu(+pfc)_3(p\text{-dpeb})]_n$ and $[Eu(+hfc)_3(p\text{-dpeb})]_n$ were classified as Λ form (Figure 2a and 2b). The dihedral angles θ of planes A (O1, C1, and C2 atoms in Figure 2c) and B (O2, C2, and C3 atoms in Figure 2c) are listed in Table 2. The dihedral angles θ in $[Eu(+hfc)_3(p\text{-dpeb})]_n$ (β-diketonate 4, 5, 6) were larger than those in $[Eu(+pfc)_3(p\text{-dpeb})]_n$ (β-diketonate 1, 2, 3). These large dihedral angles of $[Eu(+hfc)_3(p\text{-dpeb})]_n$ indicate large β-diketonate plane distortion.

Table 2. Dihedral angles of the camphorate ligands.

Compounds		Dihedral angles θ / deg.
$[Eu(+pfc)_3(p\text{-dpeb})]_n$	β-diketonate 1	2.92
	β-diketonate 2	2.35
	β-diketonate 3	5.10
	average	3.46
$[Eu(+hfc)_3(p\text{-dpeb})]_n$	β-diketonate 4	11.68
	β-diketonate 5	6.67
	β-diketonate 6	5.39
	average	6.91

Luminescence properties

The emission spectra of the chiral Eu(III) coordination polymers in the solid state are shown in Figure 3a. The emission spectra were normalized with the area of the $^5D_0 \rightarrow {}^7F_1$ transition band, which is known to be insensitive to the surrounding environment of the Eu(III) ion.[23] The emission bands at approximately 580, 590, 615, 650, and 700 nm were assigned to the 4f-4f transitions of Eu(III) ($^5D_0 \longrightarrow {}^7F_J$: J = 0, 1, 2, 3, and 4).[24]

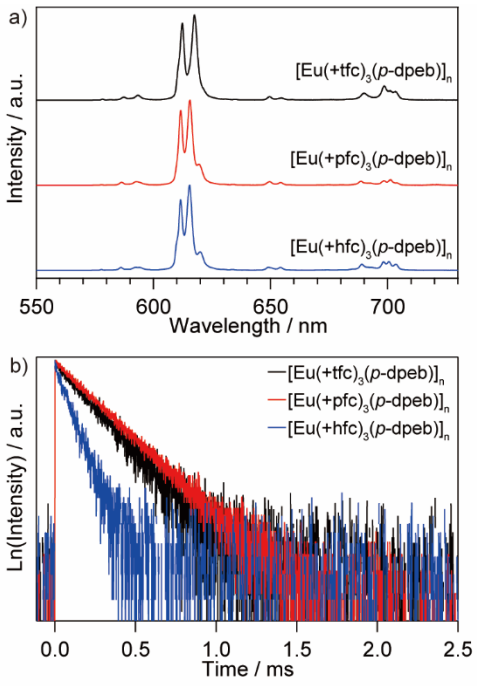

Figure 3. a) Emission spectra (λ_{ex} = 360 nm) and b) time-resolved emission decay profiles (λ_{ex} = 355 nm) of $[Eu(+tfc)_3(p\text{-dpeb})]_n$ (black), $[Eu(+pfc)_3(p\text{-dpeb})]_n$ (red), and $[Eu(+hfc)_3(p\text{-dpeb})]_n$ (blue) in the solid state measured at room temperature.

The emission band of $^5D_0 \rightarrow {}^7F_2$ transition, which is directly related to the coordination geometrical symmetry, are also shown in Figure S5b (ESI).[25] The Stark splitting of the $^5D_0 \rightarrow {}^7F_2$ transition in $[Eu(+pfc)_3(p\text{-dpeb})]_n$ is the same as that in $[Eu(+hfc)_3(p\text{-dpeb})]_n$. The coordination geometry of $[Eu(+pfc)_3(p\text{-dpeb})]_n$ is identical to that of $[Eu(+hfc)_3(p\text{-dpeb})]_n$. On the other hand, the Stark splitting of $[Eu(+tfc)_3(p\text{-dpeb})]_n$ is different from those in $[Eu(+pfc)_3(p\text{-dpeb})]_n$ and $[Eu(+hfc)_3(p\text{-dpeb})]_n$.

The emission decay profiles of the chiral Eu(III) coordination polymers in the solid state measured at room temperature are shown in Figure 3b. Single-exponential decays with sub-milli second scale lifetimes were observed. The emission lifetimes were estimated using an exponential function and are summarized in Table 3. Based on the emission lifetimes and spectra, the 4f-4f emission quantum yield ($\Phi_{f\text{-}f}$), radiative rate constant (k_r), and non-radiative rate constant (k_{nr}) were estimated using the following equations:

$$k_r = \frac{1}{\tau_{rad}} = A_{MD,0} n^3 \frac{I_{tot}}{I_{MD}} \quad (1)$$

$$\Phi_{f\text{-}f} = \frac{k_r}{k_r + k_{nr}} = \frac{\tau_{obs}}{\tau_{rad}} \quad (2)$$

$$k_{nr} = \frac{1}{\tau_{obs}} - \frac{1}{\tau_{rad}} \quad (3)$$

where τ_{obs} and τ_{rad} are the observed and radiative emission lifetimes, respectively. τ_{rad} is defined as the ideal emission lifetime without a non-radiative process. Parameters $A_{MD,0}$, n, and the calculated I_{tot}/I_{MD} are the spontaneous emission probability for the $^5D_0 \rightarrow {}^7F_1$ transition *in vacuo* (14.65 s^{-1}), refractive index of the medium (n = 1.5), and ratio of the total area of the corrected Eu(III) emission spectrum to the area of the $^5D_0 \rightarrow {}^7F_1$ band, respectively.[26]

The k_r value of the chiral Eu(III) coordination polymer with large structural strain, $[Eu(+hfc)_3(p\text{-dpeb})]_n$, is the same as those of $[Eu(+tfc)_3(p\text{-dpeb})]_n$ and $[Eu(+pfc)_3(p\text{-dpeb})]_n$. The magnitude of the k_r enhancement by the LMCT perturbation in $[Eu(+hfc)_3(p\text{-dpeb})]_n$ is similar to those in $[Eu(+tfc)_3(p\text{-dpeb})]_n$ and $[Eu(+pfc)_3(p\text{-dpeb})]_n$. On the other hand, the k_{nr} values of the chiral Eu(III) coordination polymers (1.5×10^3–7.1×10^3 s^{-1}) were strongly dependent on the substituents of the chiral camphorate ligands (+tfc, +pfc, and +hfc). The drastic changes in the k_{nr} values were derived from the LMCT quenching process. This LMCT quenching leads to decreases in both the emission lifetimes and $\Phi_{f\text{-}f}$ values.

Table 3. Photophysical parameters of chiral Eu(III) coordination polymers.

Compounds	k_r / s^{-1}	k_{nr} / s^{-1}	τ_{obs}[a] / ms	$\Phi_{f\text{-}f}$ / %
$[Eu(+tfc)_3(p\text{-dpeb})]_n$	1.2×10^3	2.0×10^3	0.31	37
$[Eu(+pfc)_3(p\text{-dpeb})]_n$	1.2×10^3	1.5×10^3	0.37	43
$[Eu(+hfc)_3(p\text{-dpeb})]_n$	1.2×10^3	7.1×10^3	0.12	15

[a] λ_{ex} = 355 nm.

Theoretical calculations

TD-DFT calculations were performed to estimate the LMCT characteristics in $[Eu(+pfc)_3(p\text{-dpeb})]_n$ and $[Eu(+hfc)_3(p\text{-dpeb})]_n$. These calculations were based on the structural parameters obtained by single-crystal X-ray structural analyses. The selected molecular orbitals of $[Eu(+pfc)_3(p\text{-dpeb})]_n$ and $[Eu(+hfc)_3(p\text{-dpeb})]_n$ are shown in Figure 4a. The calculated HOMO and LUMO are located in the camphorate ligands and Eu(III), respectively. The excitation energies and oscillator strengths of the lowest LMCT transition (π (camphorate ligand)→4*f*′ (Eu)) are summarized in Table 4. The LMCT excitation energy of $[Eu(+hfc)_3(p\text{-dpeb})]_n$ (20,810 cm^{-1}) is lower than that of $[Eu(+pfc)_3(p\text{-dpeb})]_n$ (22,530 cm^{-1}). The calculated energy levels of $[Eu(+hfc)_3(p\text{-dpeb})]_n$ and $[Eu(+pfc)_3(p\text{-dpeb})]_n$ are qualitatively consistent with the results of diffuse reflection measurements (ESI: Figure S7). The absorption edge of $[Eu(+hfc)_3(p\text{-dpeb})]_n$ (c.a. 400 nm) is longer than that of $[Eu(+tfc)_3(p\text{-dpeb})]_n$ and $[Eu(+pfc)_3(p\text{-dpeb})]_n$ (c.a. 380 nm). These lower LMCT excited states lead to energy transfer between Eu(III) and the LMCT state, resulting in a decrease of the emission quantum yield ($\Phi_{f\text{-}f}$). We also calculated the moment angle between the transition electric dipole moments of the LMCT ($\vec{\mu}_{LMCT}$) and C_4 axis in the 8-SAP structure (θ_{LMCT}, Figure 4b and Table 4). The results revealed that the θ_{LMCT} of $[Eu(+hfc)_3(p\text{-dpeb})]_n$ (79.3°) is smaller than that of $[Eu(+pfc)_3(p\text{-dpeb})]_n$ (82.5°), indicating that the bulky substituents in $[Eu(+hfc)_3(p\text{-dpeb})]_n$ affected the direction of the transition electric dipole moments.

Additionally, we performed structural optimization of $[Eu(+tfc)_3(p\text{-dpeb})_2]$ unit by DFT calculations to estimate the

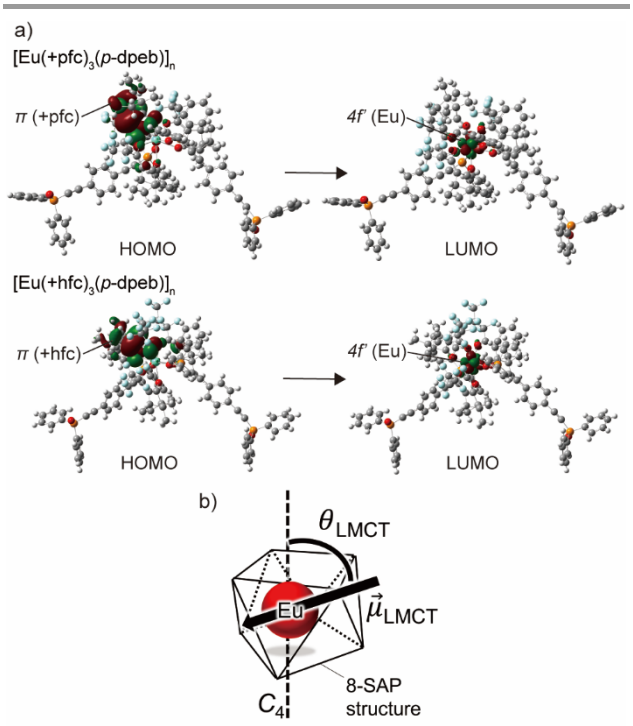

Figure 4. a) Selected α-spin molecular orbitals of $[Eu(+pfc)_3(p\text{-dpeb})]_n$ and $[Eu(+hfc)_3(p\text{-dpeb})]_n$. b) Illustration of θ_{LMCT}.

Table 4. Characteristics of the LMCT states and the energy of T_1 states obtained by TD-DFT calculations[a].

Compounds	Excitation energies of the lowest LMCT states / cm^{-1}	Oscillator strengths	θ_{LMCT} / deg.	Energy levels of T_1 states / cm^{-1}
$[Eu(+tfc)_3(p\text{-dpeb})]_n$[b]	22,310	0.0046	84.0	20,400
$[Eu(+pfc)_3(p\text{-dpeb})]_n$[c]	22,530	0.0043	82.5	20,300
$[Eu(+hfc)_3(p\text{-dpeb})]_n$[c]	20,810	0.0050	79.3	20,110

[a] TD-DFT LC-BLYP / Stuttgart RSC 1997 (for Eu atoms), cc-pVDZ (for C, H, O, F, and P atoms). [b] Based on the structure obtained by structural optimization of $[Eu(+tfc)_3(p\text{-dpeb})_2]$. [c] Based on the structure obtained by single-crystal X-ray structural analyses.

structure of $[Eu(+tfc)_3(p\text{-dpeb})]_n$. The optimized structure and the cartesian coordinates of $[Eu(+tfc)_3(p\text{-dpeb})_2]$ are shown in Figure S8 and Table S3 (ESI), respectively. The LMCT characteristics of $[Eu(+tfc)_3(p\text{-dpeb})]_n$ were also evaluated using TD-DFT calculations based on the optimized structure. The characteristics of the LMCT states were summarized in Table 4. The LMCT excitation energy of $[Eu(+tfc)_3(p\text{-dpeb})]_n$ (22,310 cm^{-1}) is similar to that of $[Eu(+pfc)_3(p\text{-dpeb})]_n$ (22,530 cm^{-1}). The θ_{LMCT} of $[Eu(+tfc)_3(p\text{-dpeb})]_n$ (84.0°) is larger than that of $[Eu(+pfc)_3(p\text{-dpeb})]_n$ and $[Eu(+hfc)_3(p\text{-dpeb})]_n$. We found that the structural strain of the camphorate ligands was closely related to the characteristics of the LMCT excited states in the chiral Eu(III) coordination polymers.

The energy level of T_1 states, which are strongly related to the energy transfer process of Eu(III) complexes,[27] are also estimated (Table 4). The T_1 energy level of $[Eu(+hfc)_3(p\text{-dpeb})]_n$ (20,110 cm^{-1}) is similar to those of $[Eu(+tfc)_3(p\text{-dpeb})]_n$ (20,400 cm^{-1}) and $[Eu(+pfc)_3(p\text{-dpeb})]_n$ (20,300 cm^{-1}). From these results, the drastically change of $\Phi_{f\text{-}f}$ is mainly caused by the LMCT excited states.

CPL properties

The CPL is characterized by the differential emission of left- and right-handed circularly polarized light.[28,29] The magnitude of the CPL (dissymmetry factors of CPL: g_{CPL}) is defined as

$$g_{CPL} = \frac{2(I_L - I_R)}{I_L + I_R} \quad (4)$$

where I_L and I_R are the intensities of the left- and right-handed circularly polarized light, respectively.[29,30] The g_{CPL} can also be represented using the transition electric and magnetic dipole moments of the f-f transition ($\vec{\mu}_{f-f}$ and $\vec{m}_{f-f}$) as follows

$$g_{CPL} = 4\frac{|\vec{\mu}_{f-f}||\vec{m}_{f-f}|\cos\theta_{\mu,m}}{|\vec{\mu}_{f-f}|^2 + |\vec{m}_{f-f}|^2} \quad (5)$$

where $\theta_{\mu,m}$ is the moment angle between the $\vec{\mu}_{f-f}$ and $\vec{m}_{f-f}$ vectors.[29,30] In the case of the Eu(III) luminophore, the magnetic dipole allowed transition ($^5D_0 \rightarrow {}^7F_1$) often provides a large $|g_{CPL}|$ value.[30–34]

The CPL spectra of the chiral Eu(III) coordination polymers in the solid state (in KBr pellets) are shown in Figure 5. Characteristic CPL signals were observed at approximately 590 ($^5D_0 \rightarrow {}^7F_1$) and 615 nm ($^5D_0 \rightarrow {}^7F_2$). The g_{CPL} values of each transition band are summarized in Table 5. The CPL signal intensities of $[Eu(+pfc)_3(p\text{-dpeb})]_n$ (g_{CPL} = −0.10) and $[Eu(+hfc)_3(p\text{-dpeb})]_n$ (g_{CPL} = −0.22) were larger than that of $[Eu(+tfc)_3(p\text{-dpeb})]_n$ (g_{CPL} = −0.05). Three types of enantiomeric coordination polymers, $[Eu(-tfc)_3(p\text{-dpeb})]_n$, $[Eu(-pfc)_3(p\text{-dpeb})]_n$, and $[Eu(-hfc)_3(p\text{-dpeb})]_n$ showed mirror images in the CPL spectra (ESI Figure S9). The enhancement of the $|g_{CPL}|$ values in both $^5D_0 \rightarrow {}^7F_1$ and $^5D_0 \rightarrow {}^7F_2$ transitions can be explained by the *J*-mixing between $^7F_1$ and $^7F_2$ sublevels.[35] The *J*-mixing is estimated by the Stark splitting energy of magnetic dipole transition band ($^5D_0 \rightarrow {}^7F_1$).[36,37] In the emission band of $^5D_0 \rightarrow {}^7F_1$ transition, the Stark splitting energies of $[Eu(+pfc)_3(p\text{-dpeb})]_n$ and $[Eu(+hfc)_3(p\text{-dpeb})]_n$ were larger than that of $[Eu(+tfc)_3(p\text{-dpeb})]_n$ (Figure S5a, ESI). The large $|g_{CPL}|$ of $[Eu(+pfc)_3(p\text{-dpeb})]_n$ and $[Eu(+hfc)_3(p\text{-dpeb})]_n$ are caused by large *J*-mixing effect. Indeed, the $|g_{CPL}|$ value of $[Eu(+hfc)_3(p\text{-}$

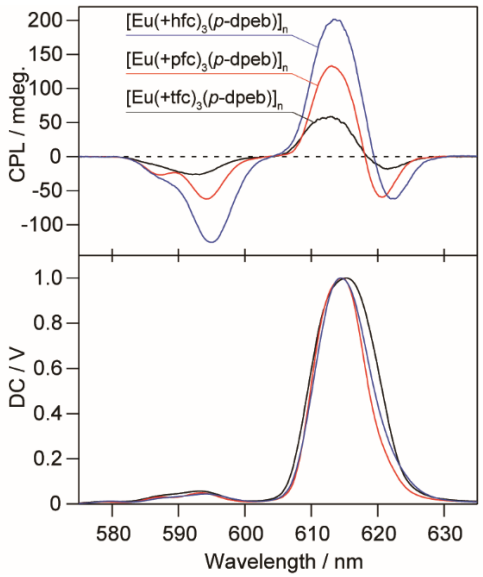

Figure 5. CPL (upper) and emission (lower) spectra (λ_{ex} = 350 nm) of $[Eu(+tfc)_3(p\text{-dpeb})]_n$ (black), $[Eu(+pfc)_3(p\text{-dpeb})]_n$ (red) and $[Eu(+hfc)_3(p\text{-dpeb})]_n$ (blue) in KBr pellet.

Table 5. The g_{CPL} values of the chiral Eu(III) coordination polymers in their $^5D_0 \rightarrow {}^7F_1$ and $^5D_0 \rightarrow {}^7F_2$transitions.

Compounds	g_{CPL} ($^5D_0 \rightarrow {}^7F_1$)	g_{CPL} ($^5D_0 \rightarrow {}^7F_2$)
$[Eu(+tfc)_3(p\text{-dpeb})]_n$	−0.05	+0.005
$[Eu(+pfc)_3(p\text{-dpeb})]_n$	−0.10	+0.010
$[Eu(+hfc)_3(p\text{-dpeb})]_n$	−0.22	+0.017

dpeb)]$_n$ was twice that of [Eu(+pfc)$_3$(*p*-dpeb)]$_n$ in both the $^5D_0 \rightarrow {}^7F_1$ and $^5D_0 \rightarrow {}^7F_2$ transitions. The Stark splitting energy and k_r value of [Eu(+hfc)$_3$(*p*-dpeb)]$_n$ are the same as those of [Eu(+pfc)$_3$(*p*-dpeb)]$_n$, resulting in constant $|\vec{\mu}_{f-f}|^2 + |\vec{m}_{f-f}|^2$ and $|\vec{\mu}_{f-f} / \vec{m}_{f-f}|$ units in equation (5). From these results, we considered that the enhanced $|g_{CPL}|$ value of [Eu(+hfc)$_3$(*p*-dpeb)]$_n$ is caused by the change in $\cos\theta_{\mu,m}$. The moment angle of $\vec{\mu}_{f-f}$ is affected by $\vec{\mu}_{LMCT}$ through LMCT perturbation, which is related to the change in $\theta_{\mu,m}$. Thus, the steric hindrance control in camphorate ligands of chiral Eu(III) coordination polymers is one of the important factors for enhancing their CPL properties.

Conclusion

Three types of chiral Eu(III) coordination polymers, [Eu(+tfc)$_3$(*p*-dpeb)]$_n$, [Eu(+pfc)$_3$(*p*-dpeb)]$_n$, and [Eu(+hfc)$_3$(*p*-dpeb)]$_n$ were synthesized. The structural distortion of [Eu(+hfc)$_3$(*p*-dpeb)]$_n$ was larger than that of [Eu(+pfc)$_3$(*p*-dpeb)]$_n$. The large structural strain affects the direction of the transition dipole moments and leads to a large $|g_{CPL}|$ value. Previously, we reported on the photophysical relationship between the LMCT states and $|g_{CPL}|$ value.[17] In this study, we successfully observed that the electronic structure of the ligands in a chiral Eu(III) coordination polymer is directly linked to the characteristics of the LMCT excited states and $|g_{CPL}|$ value. The precise tuning of the structural distortion of the chiral ligands can enhance the $|g_{CPL}|$ value for optical applications. The relationship between the CPL properties and LMCT excited states in chiral Eu(III) compounds provides novel insights in the fields of lanthanide chemistry, coordination chemistry, and photophysical science.

Experimental

Materials and methods

Materials. (+)-3-(Trifluoroacetyl)camphor (98%) and (+)-3-(heptafluorobutyryl)camphor (96%) were purchased from Sigma-Aldrich Co. LLC. (+)-Camphor (> 98.0%) was purchased from Tokyo Chemical Industry Co., Ltd. Europium(III) acetate *n*-hydrate (99.9%) was purchased from FUJIFILM Wako Pure Chemical Corporation. All other reagents were reagent grade and used without further purification.

General methods. Fourier transform infrared spectra were recorded on a JASCO FT/IR-4600 spectrometer. ESI-MS spectra were measured using a JEOL JMS-T100LP and Thermo Scientific Exactive. Elemental analyses were performed on an Exeter Analytical CE440. ^{1}H NMR (400 MHz), ^{19}F NMR (376 MHz), and ^{31}P NMR (162 MHz) spectra were recorded on a JEOL ECS400, JEOL ECZ400S, and JEOL ECX400 at 298 K, respectively. Tetramethylsilane (δ_H = 0.00 ppm), hexafluorobenzene (δ_F = −164.9 ppm), and phosphoric acid (δ_P = 0.00 ppm) were used as references for ^{1}H, ^{19}F, and ^{31}P NMR, respectively. Triple resonance ^{13}C {^{1}H, ^{19}F} NMR (151 MHz) spectrum was recorded on a JEOL JNM-ECZR equipped with a ROYAL-HFX probe. Powder X-ray diffractometry was performed on a Rigaku SmartLab using Cu-Kα radiation (λ = 1.5418 Å).

Synthetic procedures

Preparation of 1,4-bis(diphenylphosphorylethynyl)benzene (*p*-dpeb). *p*-dpeb was prepared with the procedure described in a previous report.[18]

^{1}H NMR ($CDCl_3$): δ = 7.85-7.92 (m, 8H), 7.60 (s, 4H), 7.55-7.59 (m, 4H), 7.48-7.54 ppm (m, 8H). ^{31}P NMR ($CDCl_3$): δ = 9.05 ppm. IR (ATR): ν = 3030-3076 (st, ArC-H), 2180 (st, C≡C), 1121 cm^{-1} (st, P=O). ESI-MS (*m*/*z*): $[M+H]^+$ calcd. for $C_{34}H_{25}O_2P_2$, 527.13; found, 527.13. Elemental analysis: calcd. for $C_{34}H_{24}O_2P_2$, C 77.56, H 4.59; found, C 77.44, H 4.49%.

Preparation of (+)-3-(pentafluoropropionyl)camphor. (+)-Camphor (3.0 g, 20 mmol) and sodium hydride (60% dispersion in paraffin liquid, 2.1 g) were dissolved in tetrahydrofuran (super dehydrated, 30 mL) under argon atmosphere. The mixture was stirred 30 min at room temperature, after which ethylpentafluoropropionate (3.3 mL) was dropwised to the solution at 0 °C. The mixture was stirred 10 min and refluxed for 20 h. The dark brown reaction solution was cooled to room temperature and methanol was added to consume the excess sodium hydride. Hydrochloric acid (1 mol L^{-1}, 60 mL) was added to the mixture. The product was extracted with ethyl acetate and washed with brine. The extracts were dried over anhydrous Na_2SO_4 and evaporated to give a deep red oil. The crude material was purified silica gel (Silica gel 60N, spherical neutral, particle size 100-210 μm, Kanto Chemical Co., Inc.) column chromatography (ethyl acetate: *n*-hexane = 1:5) to afford light red liquid. The liquid was further purified by distillation which gave colourless liquid.

Yield: 2.1 g (7.1 mmol, 36%). ^{1}H NMR ($CDCl_3$): δ = 11.73 (br, 1H), 2.81-2.95 (m, 1H), 2.02-2.15 (m, 1H), 1.69-1.86 (m, 1H), 1.37-1.55 (m,2H), 1.02 (s, 3H), 0.97 (s, 3H), 0.83 ppm (s, 3H). ^{13}C NMR ($CDCl_3$): δ = 214.0, 148.3, 120.2, 118.4, 109.3, 58.0, 49.0, 47.3, 30.0, 26.6, 20.3, 18.2, 8.5 ppm. ^{19}F NMR ($CDCl_3$): δ = −86.9, −124.4 ppm. ESI-MS (*m*/*z*): $[M-H]^-$ calcd. for $C_{13}H_{15}F_5O_2$, 297.09; found, 297.09.

Preparation of [Eu(+tfc)$_3$(*p*-dpeb)]$_n$. Europium(III) acetate *n*-hydrate (0.36 g) was dissolved in distilled water (150 mL). (+)-3-Triflouroacetylcamphor (0.50 g, 2.0 mmol) in methanol (15 mL) was added to the solution, and the mixture was stirred for 4 h at room temperature. The obtained powder was washed with distilled water, and the powder was dried in vacuo ([Eu(+tfc)$_3$(H_2O)$_2$], 0.41 g). [Eu(+tfc)$_3$(H_2O)$_2$] (0.37 g, 0.40 mmol) and *p*-dpeb (0.18 g, 0.33 mmol) were dissolved in methanol (10 mL) and refluxed for 5 h. The reaction mixture was cooled to room temperature and evaporated to give a light yellow powder. The obtained powder was washed with diethyl ether and recrystallized from ethanol to give light yellow powder.

Yield: 35% for monomer. IR (ATR): 2865-2990 (st, ArC-H), 2183 (st, C≡C), 1660 (st, C=O), 1120 (st, P=O). ESI-MS (*m*/*z*): $[M-tfc]^+$ calcd. for $C_{58}H_{52}EuF_6O_6P_2$, 1173.24; found, 1173.25. Elemental analysis: calcd. for $C_{70}H_{66}EuF_9O_8P_2$, C 59.20, H 4.68; found, C 58.87, H 4.57%.

Preparation of [Eu(+pfc)$_3$(*p*-dpeb)]$_n$. Europium(III) acetate *n*-hydrate (0.42 g) was dissolved in distilled water (150 mL). (+)-3-(Pentafluoropropionyl)camphor (0.71 g, 2.4 mmol) in methanol (20 mL) was added to the solution, and the mixture was stirred for 18 h at room temperature. The obtained powder was washed with distilled water, and the powder was dried in vacuo ([Eu(+pfc)$_3$(H$_2$O)$_n$, 0.56 g). [Eu(+pfc)$_3$(H$_2$O)$_n$] (0.11 g) and *p*-dpeb (62 mg, 0.12 mmol) were dissolved in methanol (10 mL) and refluxed for 20 h. The reaction mixture was cooled to room temperature and evaporated to give a light yellow powder. The obtained powder was recrystallized from ethanol to give light yellow powder.
Yield: 53 mg (0.034 mmol, 28%; for monomer). IR (ATR): 2868-2995 (st, ArC-H), 2183 (st, C≡C), 1654 (st, C=O), 1126 (st, P=O). ESI-MS (*m*/*z*): [M−pfc]$^+$ calcd. for $C_{60}H_{52}EuF_{10}O_6P_2$, 1273.23; found, 1273.22. Elemental analysis: calcd. for $C_{73}H_{66}EuF_{15}O_8P_2$, C 55.84, H 4.24; found, C 55.63, H 4.11%.

Preparation of [Eu(+hfc)$_3$(*p*-dpeb)]$_n$: Europium(III) acetate *n*-hydrate (0.38 g) was dissolved in distilled water (200 mL), and a few drops of 28% ammonia solution were added (pH = 8). (+)-3-(Heptafluorobutyryl)camphor (1.1 g, 3.2 mmol) in methanol (40 mL) was added to the solution, and the mixture was stirred for 22 h at room temperature. The obtained powder was washed with distilled water, and the powder was dried in vacuo ([Eu(+hfc)$_3$(H$_2$O)$_n$, 0.94 g). [Eu(+hfc)$_3$(H$_2$O)$_n$] (78 mg) and *p*-dpeb (40 mg, 0.08 mmol) were dissolved in methanol (10 mL) and refluxed for 5 h. The reaction solution was cooled to room temperature and evaporated to give a light yellow powder. The obtained powder was recrystallized from ethanol to give light yellow powder.
Yield: 37 mg (0.022 mmol, 27%; for monomer). IR (ATR): 2870-2999 (st, ArC-H), 2183 (st, C≡C), 1652 (st, C=O), 1187 (st, P=O). ESI-MS (*m*/*z*): [M−hfc]$^+$ calcd. for $C_{62}H_{52}EuF_{14}O_6P_2$, 1373.22; found, 1373.22. Elemental analysis: calcd. for $C_{76}H_{66}EuF_{21}O_8P_2$, C 53.06, H 3.87; found, C 52.85, H 3.75%.

Optical Measurements

Emission and excitation spectra were recorded on a HORIBA Fluorolog-3 spectrofluorometer and corrected for the response of the detector system. Emission decay profiles were measured using the third harmonics (355 nm) of a Q-switched Nd:YAG laser (Spectra Physics, INDI-50, FWHM = 5 ns, λ = 1064 nm) and a photomultiplier (Hamamatsu Photonics, R5108, response time ≤ 1.1 ns). The Nd:YAG laser response was monitored with a digital oscilloscope (Sony Tektronix, TDS3052, 500 MHz) synchronized to the single-pulse excitation. Emission lifetimes were determined from the slope of logarithmic plots of the decay profiles. Emission lifetimes in the range of 150–370 K were measured using a cryostat (Thermal Block Company, SA-SB245T) and a temperature controller (Oxford, Instruments, ITC 502S). Diffuse reflection spectra were measured using a JASCO V-770 spectrophotometer with an ISN-923 integrating sphere unit. CPL spectra were recorded on a JASCO CPL-300 spectro-fluoropolarimeter for Eu(III) coordination polymers (0.5 mg) mixed with KBr (150 mg). KBr tablets (diameter: 10 mm, Eu(III) coordination polymers / KBr) were prepared using a PT-10 tablet forming machine (48.2 kN, press time: 3 min).

Crystallography

Single crystals of [Eu(+pfc)$_3$(*p*-dpeb)]$_n$ and [Eu(+hfc)$_3$(*p*-dpeb)]$_n$ were obtained by the recrystallization from ethanol solution. The single crystal X-ray structural analyses were carried out using Rigaku XtaLAB Synergy-R/DW equipped with a HyPix-6000HE detector (MoKα radiation, λ = 0.71073 Å). The structure was solved by direct methods and expanded using Fourier techniques. Non-hydrogen atoms were refined anisotropically using the SHELX system.[38] Hydrogen atoms were refined using the riding model. All calculations were performed using the crystal structure crystallographic and Olex 2 software package.[39] The CIF data were confirmed by the checkCIF/PLATON service. CCDC 2213525 (for [Eu(+pfc)$_3$(*p*-dpeb)]$_n$) and 2213526 (for [Eu(+hfc)$_3$(*p*-dpeb)]$_n$) contain the supplementary crystallographic data for this paper. These data can be obtained free of charge from The Cambridge Crystallographic Data Centre via www.ccdc.cam.ac.uk/structures/

Computational Details

All quantum chemical calculations were performed by the density functional theory (DFT) using the Gaussian 16 package.[40] Structural optimization was carried out using DFT with B3LYP-D3 functional[41–43] (basis set: Stuttgart RSC 1997 (ECP28MWB)[44,45] for Eu atom and 6-31G(d) for other elements). The excited states were investigated using time-dependent (TD)-DFT with the long-range corrected LC-BLYP functional.[46] The spin-unrestricted self-consistent field calculations were performed. The Stuttgart RSC 1997 (ECP28MWB) basis set was adopted for Eu atoms, while the cc-pVDZ basis set[47] was used for the other atoms.

Author contributions

M.T. performed all the syntheses, photophysical measurements, X-ray analyses, quantum chemical calculations and wrote the paper. Y.K., S.S., K.F., and Y.H. discussed and designed the research. All authors reviewed the manuscript and approved the final version.

Conflicts of interest

The authors declare no competing financial interest.

Acknowledgements

This work was supported by JSPS KAKENHI Grants Number JP20K21201 (Y.H.), JP22H02152 (Y.H), JP22H04516 (Y.H), JP20H02748 (Y.K.), JP21K18969 (Y.K.), JP22K14741 (S.S.) of the Ministry of Education, Culture, Sports, Science, and Technology (MEXT) of Japan. This work was also supported by the Institute for Chemical Reaction Design and Discovery (ICReDD), established by the World Premier International Research Center Initiative (WPI) and Grant-in-Aid for JSPS Fellows Grants

Number JP21J20980 (M.T.) of MEXT, Japan. The authors express sincere thanks to Prof. H. Ito and Dr. M. Jin from Hokkaido University for experimental assistance.

Notes and references

1 Y. He, Z. Huang, K. Wu, J. Ma, Y. G. Zhou and Z. Yu, Recent advances in transition-metal-catalyzed carbene insertion to C-H bonds, *Chem. Soc. Rev.*, 2022, **51**, 2459–2852.

2 K. P. S. Cheung, S. Sarkar and V. Gevorgyan, Visible Light-Induced Transition Metal Catalysis, *Chem. Rev.*, 2022, **122**, 1543–1625.

3 M. Irikura, Y. Tamaki and O. Ishitani, Development of a panchromatic photosensitizer and its application to photocatalytic CO2 reduction, *Chem. Sci.*, 2021, **12**, 13888–13896.

4 P. Xu, P. López-Rojas and T. Ritter, Radical Decarboxylative Carbometalation of Benzoic Acids: A Solution to Aromatic Decarboxylative Fluorination, *J. Am. Chem. Soc.*, 2021, **143**, 5349–5354.

5 Q. Pan, M. Abdellah, Y. Cao, W. Lin, Y. Liu, J. Meng, Q. Zhou, Q. Zhao, X. Yan, Z. Li, H. Cui, H. Cao, W. Fang, D. A. Tanner, M. Abdel-Hafiez, Y. Zhou, T. Pullerits, S. E. Canton, H. Xu and K. Zheng, Ultrafast charge transfer dynamics in 2D covalent organic frameworks/Re-complex hybrid photocatalyst, *Nat. Commun.*, 2022, **13**, 845.

6 A. Ilic, J. Schwarz, C. Johnson, L. H. M. de Groot, S. Kaufhold, R. Lomoth and K. Wärnmark, Photoredox catalysis via consecutive ^{2}LMCT- and ^{3}MLCT-excitation of an Fe(iii / ii)–N-heterocyclic carbene complex, *Chem. Sci.*, 2022, **13**, 9165–9175.

7 M. Wang and K. Ishii, Photochemical properties of phthalocyanines with transition metal ions, *Coord. Chem. Rev.*, 2022, **468**, 214626.

8 T. Kinoshita, M. Otsubo, T. Ono and H. Segawa, Enhancement of Near-Infrared Singlet-Triplet Absorption of Ru(II) Sensitizers for Improving Conversion Efficiency of Solar Cells, *ACS Appl. Energy Mater.*, 2021, **4**, 7052–7063.

9 R. Mishra, K. Jain, V. P. Sharma, S. Kishor and L. M. Ramaniah, Heteroleptic Cu(i) bis-diimine complexes as sensitizers in dye-sensitized solar cells (DSSCs): on some factors affecting intramolecular charge transfer, *Phys. Chem. Chem. Phys.*, 2022, **24**, 17217–17232.

10 T. Kuwahara, H. Ohtsu and K. Tsuge, Synthesis and Photophysical Properties of Emissive Silver(I) Halogenido Coordination Polymers Composed of $\{Ag_2X_2\}$ Units Bridged by Pyrazine, Methylpyrazine, and Aminopyrazine, *Inorg. Chem.*, 2021, **60**, 1299–1304.

11 A. Alconchel, O. Crespo and M. Concepción Gimeno, Versatile Emissive Three-Coordinated Gold(I) Systems-Properties and Perspectives, *Eur. J. Inorg. Chem.*, 2021, **2021**, 3913–3925.

12 H. C. London, D. Y. Pritchett, J. A. Pienkos, C. D. Mcmillen, T. J. Whittemore, C. J. Bready, A. R. Myers, N. C. Vieira, S. Harold, G. C. Shields and P. S. Wagenknecht, Photochemistry and Photophysics of Charge-Transfer Excited States in Emissive d^{10}/d^{0} Heterobimetallic Titanocene Tweezer Complexes, *Inorg. Chem.*, 2022, **61**, 10986–10998.

13 P. Herr, C. Kerzig, C. B. Larsen, D. Häussinger and O. S. Wenger, Manganese(i) complexes with metal-to-ligand charge transfer luminescence and photoreactivity, *Nat. Chem.*, 2021, **13**, 956–962.

14 C. K. Jørgensen, Electron transfer spectra of lanthanide complexes, *Mol. Phys.*, 1962, **5**, 271–277.

15 Y. Kitagawa, P. P. Ferreira Da Rosa and Y. Hasegawa, Charge-transfer excited states of π- And 4f-orbitals for development of luminescent Eu(iii) complexes, *Dalton Trans.*, 2021, **50**, 14978–14984.

16 M. Tsurui, Y. Kitagawa, K. Fushimi, M. Gon, K. Tanaka and Y. Hasegawa, Electronic strain effect on Eu(iii) complexes for enhanced circularly polarized luminescence, *Dalton Trans.*, 2020, **49**, 5352–5361.

17 M. Tsurui, Y. Kitagawa, S. Shoji, H. Ohmagari, M. Hasegawa, M. Gon, K. Tanaka, M. Kobayashi, T. Taketsugu, K. Fushimi and Y. Hasegawa, Asymmetric Lumino-Transformer: Circularly Polarized Luminescence of Chiral Eu(III) Coordination Polymer with Phase-Transition Behavior, *J. Phys. Chem. B*, 2022, **126**, 3799–3807.

18 Y. Hirai, T. Nakanishi, Y. Kitagawa, K. Fushimi, T. Seki, H. Ito, H. Fueno, K. Tanaka, T. Satoh and Y. Hasegawa, Luminescent Coordination Glass: Remarkable Morphological Strategy for Assembled Eu(III) Complexes, *Inorg. Chem.*, 2015, **54**, 4364–4370.

19 T. Harada, Y. Nakano, M. Fujiki, M. Naito, T. Kawai and Y. Hasegawa, Circularly Polarized Luminescence of Eu(III) Complexes with Point- and Axis-Chiral Ligands Dependent on Coordination Structures, *Inorg. Chem.*, 2009, **48**, 11242–11250.

20 D. Casanova, M. Llunell, P. Alemany and S. Alvarez, The Rich Stereochemistry of Eight-Vertex Polyhedra: A Continuous Shape Measures Study, *Chem. Eur. J.*, 2005, **11**, 1479–1494.

21 M. Pinsky and D. Avnir, Continuous Symmetry Measures. 5. The Classical Polyhedra, *Inorg. Chem.*, 1998, **37**, 5575–5582.

22 Universitat de Barcelona, "Electronic Structure Group - SHAPE 2.1", http://www.ee.ub.edu/.

23 C. Görller-Walrand, L. Fluyt, A. Ceulemans and W. T. Carnall, Magnetic dipole transitions as standards for Judd–Ofelt parametrization in lanthanide spectra, *J. Chem. Phys.*, 1991, **95**, 3099–3106.

24 K. Binnemans, Interpretation of europium (III) spectra, *Coord. Chem. Rev.*, 2015, **295**, 1–45.

25 S. Yanagida, Y. Hasegawa, K. Murakoshi, Y. Wada, N. Nakashima and T. Yamanaka, Strategies for enhancing photoluminescence of Nd^{3+} in liquid media, *Coord. Chem. Rev.*, 1998, **171**, 461–480.

26 M. H. V. V. Werts, R. T. F. F. Jukes and J. W. Verhoeven, The emission spectrum and the radiative lifetime of Eu^{3+} in luminescent lanthanide complexes, *Phys. Chem. Chem. Phys.*, 2002, **4**, 1542–1548.

27 M. Latva, H. Takalob, V. M. Mukkala, C. Matachescu, J. C. Rodríguez-Ubis and J. Kankare, Correlation between the

lowest triplet state energy level of the ligand and lanthanide(III) luminescence quantum yield, *J. Lumin.*, 1997, **75**, 149–169.

28 F. S. Richardson, J. P. Riehl, F. S. Richardson and J. P. Riehl, Circularly Polarized Luminescence Spectroscopy, *Chem. Rev.*, 1977, **77**, 773–792.

29 S. F. Mason, *Molecular optical activity and the chiral discriminations*, Cambridge University Press, 1982.

30 F. Zinna and L. Di Bari, Lanthanide Circularly Polarized Luminescence: Bases and Applications, *Chirality*, 2015, **27**, 1–13.

31 F. Zinna, M. Pasini, F. Galeotti, C. Botta, L. Di Bari and U. Giovanella, Design of Lanthanide-Based OLEDs with Remarkable Circularly Polarized Electroluminescence, *Adv. Funct. Mater.*, 2017, **27**, 1603719.

32 G. Muller, Luminescent chiral lanthanide(III) complexes as potential molecular probes, *Dalton Trans.*, 2009, 9692–9707.

33 R. Carr, N. H. Evans and D. Parker, Lanthanide complexes as chiral probes exploiting circularly polarized luminescence, *Chem. Soc. Rev.*, 2012, **41**, 7673–7686.

34 Y. Kitagawa, M. Tsurui and Y. Hasegawa, Steric and Electronic Control of Chiral Eu(III) Complexes for Effective Circularly Polarized Luminescence, *ACS Omega*, 2020, **5**, 3786–3791.

35 S. Wada, Y. Kitagawa, T. Nakanishi, M. Gon, K. Tanaka, K. Fushimi, Y. Chujo and Y. Hasegawa, Electronic chirality inversion of lanthanide complex induced by achiral molecules, *Sci. Rep.*, 2018, **8**, 1–9.

36 K. Binnemans, Interpretation of europium(III) spectra, *Coord. Chem. Rev.*, 2015, **295**, 1–45.

37 C.-G. Ma, M. G. Brik, V. Kiisk, T. Kangur and I. Sildos, Spectroscopic and crystal-field analysis of energy levels of Eu^{3+} in SnO_2 in comparison with ZrO_2 and TiO_2, *J. Alloys Compd.*, 2011, **509**, 3441–3451.

38 G. M. Sheldrick, A short history of SHELX, *Acta Crystallogr. Sect. A Found. Crystallogr.*, 2008, **64**, 112–122.

39 O. V. Dolomanov, L. J. Bourhis, R. J. Gildea, J. A. K. Howard and H. Puschmann, OLEX2: A complete structure solution, refinement and analysis program, *J. Appl. Crystallogr.*, 2009, **42**, 339–341.

40 M. J. Frisch, G. W. Trucks, H. B. Schlegel, G. E. Scuseria, M. a. Robb, J. R. Cheeseman, G. Scalmani, V. Barone, G. a. Petersson, H. Nakatsuji, X. Li, M. Caricato, a. V. Marenich, J. Bloino, B. G. Janesko, R. Gomperts, B. Mennucci, H. P. Hratchian, J. V. Ortiz, a. F. Izmaylov, J. L. Sonnenberg, Williams, F. Ding, F. Lipparini, F. Egidi, J. Goings, B. Peng, A. Petrone, T. Henderson, D. Ranasinghe, V. G. Zakrzewski, J. Gao, N. Rega, G. Zheng, W. Liang, M. Hada, M. Ehara, K. Toyota, R. Fukuda, J. Hasegawa, M. Ishida, T. Nakajima, Y. Honda, O. Kitao, H. Nakai, T. Vreven, K. Throssell, J. a. Montgomery Jr., J. E. Peralta, F. Ogliaro, M. J. Bearpark, J. J. Heyd, E. N. Brothers, K. N. Kudin, V. N. Staroverov, T. a. Keith, R. Kobayashi, J. Normand, K. Raghavachari, a. P. Rendell, J. C. Burant, S. S. Iyengar, J. Tomasi, M. Cossi, J. M. Millam, M. Klene, C. Adamo, R. Cammi, J. W. Ochterski, R. L. Martin, K. Morokuma, O. Farkas, J. B. Foresman and D. J. Fox, 2016, Gaussian 16, Revision C.01, Gaussian, Inc., Wallin.

41 Axel D. Becke1, Density-functional thermochemistry. III. The role of exact exchange, *J. Chem. Phys.*, 1993, **98**, 5648.

42 P. J. Stephens, F. J. Devlin, C. F. Chabalowski and M. J. Frisch, Ab Initio Calculation of Vibrational Absorption and Circular Dichroism Spectra Using Density Functional Force Fields, *J. Phys. Chem.*, 1994, **98**, 11623–11627.

43 S. Grimme, J. Antony, S. Ehrlich and H. Krieg, A consistent and accurate ab initio parametrization of density functional dispersion correction (DFT-D) for the 94 elements H-Pu, *J. Chem. Phys.*, 2010, **132**, 154104.

44 M. Dolg, H. Stoll, A. Savin and H. Preuss, Energy-adjusted pseudopotentials for the rare earth elements, *Theor. Chim. Acta*, 1989, **75**, 173–194.

45 B. P. Pritchard, D. Altarawy, B. Didier, T. D. Gibson and T. L. Windus, New Basis Set Exchange: An Open, Up-to-Date Resource for the Molecular Sciences Community, *J. Chem. Inf. Model.*, 2019, **59**, 4814–4820.

46 J. Da Chai and M. Head-Gordon, Long-range corrected hybrid density functionals with damped atom-atom dispersion corrections, *Phys. Chem. Chem. Phys.*, 2008, **10**, 6615–6620.

47 T. H. Dunning, Gaussian basis sets for use in correlated molecular calculations. I. The atoms boron through neon and hydrogen, *J. Chem. Phys.*, 1989, **90**, 1007–1023.